

From Bipolar to Quadrupolar Electrode Structures: An Application of Bond-Detach Lithography for Dielectrophoretic Particle Assembly

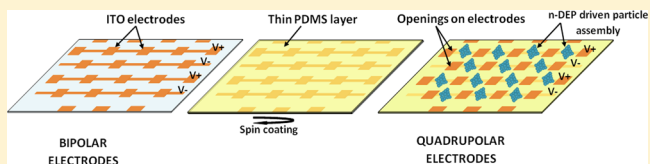
Samia Menad,[†] Amal El-Gaddar,[†] Naoufel Haddour,^{*,†} Sylvain Toru,[†] Mathieu Brun,[†] François Buret,[†] and Marie Frenea-Robin^{*,‡}

[†]Université de Lyon, Ecole Centrale de Lyon, CNRS, UMR 5005, Laboratoire Ampère, Écully, F-69130, France

[‡]Université de Lyon, Université Lyon 1, CNRS, UMR 5005, Laboratoire Ampère, Villeurbanne, F-69622, France

Supporting Information

ABSTRACT: We describe a new, simple process for fabricating transparent quadrupolar electrode arrays enabling large-scale particle assembly by means of dielectrophoresis. In the first step, interdigitated electrode arrays are made by chemical wet etching of indium tin oxide (ITO). Then, the transition from a bipolar to a quadrupolar electrode arrangement is obtained by covering the electrode surface with a thin poly(dimethylsiloxane) (PDMS) film acting as an electrical insulation layer in which selective openings are formed using bond-detach lithography. The PDMS insulating layer thickness was optimized and controlled by adjusting experimental parameters such as the PDMS viscosity (modulated by the addition of heptane) and the PDMS spin-coating velocity. The insulating character of the PDMS membrane was successfully demonstrated by performing a dielectrophoretic assembly of polystyrene particles using interdigitated electrodes with and without a PDMS layer. The results show that the patterned PDMS film functions properly as an electrical insulation layer and allows the reconfiguration of the electric field cartography. Electric field simulations were performed in both configurations to predict the dielectrophoretic behavior of the particles. The simulation results are in perfect agreement with experiments, in which we demonstrated the formation of concentrated clusters of polystyrene particles and living cells of regular size and shape.



INTRODUCTION

The dielectrophoretic phenomenon was first described by Pohl in 1951 as the translational motion of neutral matter generated by polarization effects in a nonuniform electric field.¹ Since then, dielectrophoresis (DEP) has become an increasingly popular tool for the manipulation and assembly of a wide range of colloidal particles and offers great potential for the development of functional materials from organized matter. This technique has been used for various applications such as the manipulation of living cells² and biomolecules,³ electrical characterization of colloidal particles,^{4,5} and assembly of micro and nanostructures⁶ with electronic or photonic functionality.⁷

DEP is typically carried out on planar electrode arrays obtained by patterning a conductive layer deposited on glass or silicon. Common electrode configurations used in DEP assembly are simple planar electrodes such as gap,⁸ interdigitated,⁹ and quadrupolar electrodes.¹⁰ Gap or interdigitated electrodes are commonly used to perform a massively parallel manipulation of cells or particles, as they can be arranged in large arrays that are simple to fabricate, requiring only a single photolithography step. Quadrupolar electrodes are often used to measure particle or cell properties using electrorotation.^{11–13} They are also largely employed to study the dielectrophoretic behavior of particles, as they provide a good separation between field minima and maxima, where particles are respectively collected under negative and positive DEP conditions (Figure 1). In particular, quadrupolar electrodes of polynomial design¹⁴ offer an optimal electric field

configuration for particle focusing by negative DEP^{4,5} and are therefore well adapted to the formation of particle clusters or cell aggregates.¹⁵ However, this electrode structure is rarely employed when a large manipulation area is required, since the fabrication of quadrupolar electrode matrices remains a challenge.

The fabrication of such electrode arrays requires the use of metal–insulator–metal sandwich structures resulting from several lithography steps. Electrode interconnection can be achieved by creating openings in the insulation layer, which allows the formation of vias between the two metal layers. The insulation layer is typically obtained by depositing SiO₂ or Si₃N₄ using plasma-enhanced chemical vapor deposition (PECVD)^{16,17} and patterned using HF wet etching or reactive ion etching (RIE). This fabrication method is time-consuming and requires expensive clean room facilities.

Another promising approach based on the pyroelectric effect in periodically poled lithium niobate substrates also allows large-scale dielectrophoretic particle assembly.^{18,19} In this solution, neither external circuits nor electrodes are required, but as a counterpart, the DEP phenomenon is restricted to the dc regime.

In this article, we present simple, low-cost technology for the fabrication of a transparent electronic microchip comprising a

Received: February 7, 2014

Revised: April 20, 2014

Published: April 23, 2014

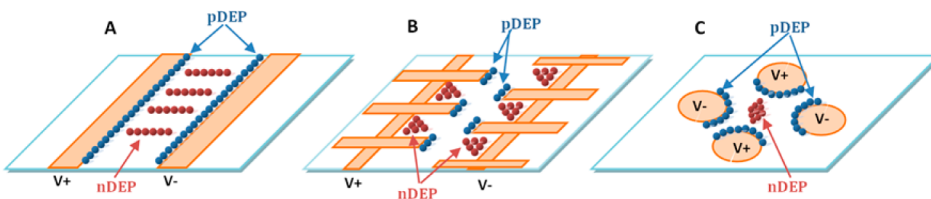


Figure 1. Electrode configurations and dielectrophoretic behavior of particles under a nonuniform ac electric field. (A) Gap electrodes, (B) interdigitated electrodes, and (C) quadrupolar electrodes.

large area of quadrupolar electrodes for colloidal particle assembly. Our approach consists in patterning a thin PDMS layer employed as an insulating film to fabricate a matrix of quadrupolar electrodes from a simple bipolar electrode array made of ITO.

It is generally agreed that PDMS is among the most popular polymeric materials employed in microelectromechanical systems (MEMS),²⁰ microfluidic devices,²¹ and biomedical chips,²² which is due to its ease of manipulation, nontoxicity, biocompatibility,²³ excellent optical transparency²⁴ and low cost. As PDMS is a nonelectrically conductive material, it may also be advantageously exploited to perform selective electrical insulation of microelectrodes.²⁵ To our knowledge, the work of Park and co-workers remains the unique example of electrode passivation using micropatterned PDMS. However, the application presented in ref 25 (culture of neuron cells on top of the patterned PDMS layer) did not show how PDMS patterning could modify the distribution of the field around the electrodes, which is particularly interesting in DEP-based applications.

While PDMS patterning remains a challenging task, different approaches were proposed in the literature, including blade scratching,²⁶ plasma etching,²⁷ parylene C lift-off,²⁸ photoresist lift-off,²⁵ and the use of photodefinable PDMS.²⁹ Blade scratching consists of pouring PDMS prepolymer over a photoresist mold before mechanically removing excess PDMS using a rubber blade, which leaves PDMS only between the photoresist walls. However, this technique is not well suited for thin PDMS layer patterning. PDMS patterning using plasma etching relies on optimized processes involving F-containing plasma such as SF₆ to lower the surface and sidewall roughness. This approach therefore requires specific equipment.

The lift-off-based techniques, requiring the use of intermediate parylene C²⁸ or photoresist²⁵ layers, may provide smooth surfaces. However, results reported in the literature were obtained using a relatively important PDMS membrane and sacrificial layer thicknesses. The reliability of the technique should depend on these parameters and has not been demonstrated in the aforementioned studies for thin PDMS membranes (<4 μm). Grilli et al. also demonstrated the direct patterning of PDMS films by modulating the wettability of polar dielectric substrates using the pyroelectric effect.³⁰ However, this technique requires the use of specific substrates, such as lithium niobate. Thangawng et al. have proposed a simple, low-cost PDMS patterning approach referred to as bond-detach lithography (BDL),³¹ which consists of using microstructured PDMS stamps to pattern ultrathin PDMS films deposited on various substrates. The performances of this approach were illustrated on silicon, photoresist-coated Si, and Teflon-coated Si substrates, which were opaque and non-conductive. The present article demonstrates how this technique could be further developed to allow its utilization on glass substrates bearing patterned ITO electrodes and

thereby to obtain selectively insulated electrode arrays. The functionality of the chip was confirmed experimentally by performing microparticle and cell assembly using negative DEP.

THEORETICAL BASIS

DEP Principle. The term DEP refers to the motion of polarizable particles resulting from the interaction of a nonuniform electric field with the induced dipole moment. The time-averaged dielectrophoretic force $\langle F_{DEP} \rangle$ exerted on a spherical particle of radius r is expressed as^{32,33}

$$F_{DEP} = 2\pi\epsilon_m r^3 Re[CM] \nabla |E|^2 \quad (1)$$

where ϵ_m is the permittivity of the particle immersion medium. E refers to the rms strength of the electric field, and $Re[CM]$ is the real part of the Clausius–Mossotti (CM) factor, which can be further expressed as

$$Re(CM) = Re\left(\frac{\tilde{\epsilon}_p - \tilde{\epsilon}_m}{\tilde{\epsilon}_p + 2\tilde{\epsilon}_m}\right) \quad (2)$$

$$\tilde{\epsilon} = \epsilon - j\frac{\sigma}{\omega} \quad (3)$$

$\tilde{\epsilon}_p$ and $\tilde{\epsilon}_m$ respectively represent the complex permittivities of the particle and media, which depend on the conductivity σ and electric field angular frequency ω .

The direction and magnitude of the DEP force therefore depend on the dielectric properties of the particle and solution and on the applied electric signal characteristics. When the polarizability of the particle is greater than that of the suspending medium ($Re(CM)>0$), the resulting DEP force directs the particle toward the strongest field region at electrode edges. This phenomenon is referred to as positive DEP (pDEP). The opposite case ($Re(CM)<0$) corresponds to negative DEP (nDEP), where the particles are repelled from strong electric field areas to the weakest electric field regions.

The dielectrophoretic behavior of particles can therefore be predicted from the knowledge of their electrical properties.

Electric Properties of Latex Beads. The conductivity of a latex microparticle is governed by its surface charge and can be approximated as³⁴

$$\sigma_p = \frac{2K_s}{r} \quad (4)$$

by neglecting the particle interior conductivity. K_s is the surface conductance, which can be expressed as the sum of two components,

$$K_s = K_s^i + K_s^d \quad (5)$$

where K_s^i and K_s^d are the Stern and diffuse layer conductance, respectively. The first component reflects the field-induced mobility of counterions strongly attracted to charges on the

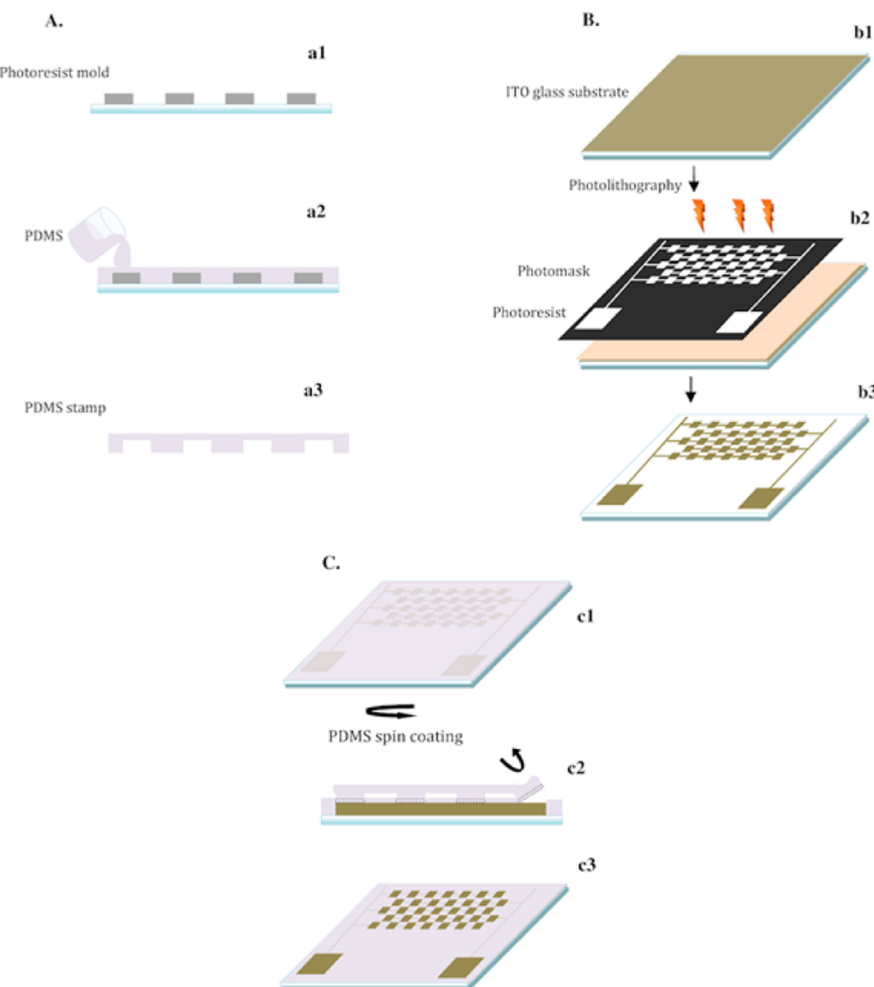


Figure 2. Fabrication steps of the microelectronic chip. (A) PDMS stamp fabrication: (a1) Photoresist mold fabrication, (a2) PDMS pouring and curing, and (a3) PDMS peeling off of the photoresist mold. (B) Bipolar ITO electrode fabrication: (b1) ITO glass substrate, (b2) negative photoresist coating and UV illumination through a mask, and (b3) photoresist development and chemical etching to remove the unexposed ITO. (C) BDL process: (c1) thin PDMS layer deposition, (c2) bonding between the PDMS stamp and the PDMS-coated ITO/glass substrate followed by peeling of the PDMS stamp, which creates openings in the thin PDMS insulating layer, and (c3) resulting ITO quadrupolar electrode matrix.

particle surface (Stern layer), and the second, that of more loosely attracted counterions in the diffuse part of the double layer.

The diffuse layer conductance is described by³⁵

$$K_s^d = \frac{4F^2cz^2D\left(1 + \frac{3m}{z^2}\right)}{RT\kappa} \left(\cosh\left[\frac{zq\zeta}{2kT}\right] - 1 \right) \quad (6)$$

where F is the Faraday constant, c is the electrolyte concentration expressed in mol m⁻³, z is the valency of the counterion, D is the ion diffusion coefficient of ζ , R is the molar gas constant, T is the temperature, and κ is the inverse Debye length, given by

$$\sqrt{\frac{2czF^2}{\epsilon_m RT}} \quad (7)$$

m is a dimensionless parameter describing the electroosmotic contribution to K_s^d , which can be determined from

$$m = \left(\frac{RT}{F}\right)^2 \frac{2\epsilon_m}{3\eta D} \quad (8)$$

where η is the medium viscosity.

The permittivity of latex particles is $\epsilon_p = 2.56 \times \epsilon_0(F/m)$, where ϵ_0 is the permittivity of vacuum.

EXPERIMENTAL SECTION

Chip Fabrication. The fabrication of the microelectronic chip is divided into three main steps, which are depicted in Figure 2. It consists of (A) PDMS stamp fabrication, (B) bipolar ITO electrode fabrication, and (C) the BDL process.

PDMS Stamp Fabrication: First, the SU-8 master mold (SU-8 2013, Micro-Chem) for the PDMS stamp was fabricated on a glass slide by photolithography. The protocol used for SU-8 negative photoresist deposition and patterning is the same as the one used for bipolar ITO electrode fabrication, described below. Once the SU-8 master mold was ready, the PDMS prepolymer solution containing a mixture (10:1 mass ratio) of PDMS oligomers and a reticular agent from Sylgard 184 kit (Dow Corning) was poured onto the master and thermally cured at 80 °C for 1 h (Figure 2A). Finally, the stamp was gently peeled off of the SU-8 master mold.

Bipolar ITO Electrode Fabrication: An interdigitated electrode array was fabricated by photolithography on an indium tin oxide-coated glass slide (8–12 Ω/sq, 25 mm × 25 mm) purchased from Sigma-Aldrich. The electrodes are composed of 150 μm × 150 μm square patterns disposed in staggered rows, with two adjacent squares being separated by a track of length 250 μm and width 30 μm. The electrode

thickness has been measured with a Dektak 3030 surface profiler and found to be 150 nm.

A layer of SU-8 was used as an etching mask for ITO patterning by wet chemical etching. First, SU-8 photoresist (SU-8 2010 Micro-Chem) was spun onto the ITO/glass slide by spin coating at 500 rpm for 8 s, followed by 3000 rpm for 60 s using a Spin 150 spin-coater (SPS). After that, the substrate was prebaked at 65 °C for 1 min and then at 95 °C for 2 min. This two-step baking process was required to avoid cracks in the SU-8 layer. The deposited photoresist was isolated for 10 s through a photomask bearing the desired electrode pattern using a UV LED masker (UV-KUB, Kloé). After exposure, the sample was postbaked at 65 °C for 1 min and at 95 °C for 2 min 30 s.

SU-8 was developed in propylene glycol methyl ether acetate (PGMEA, Sigma-Aldrich, France) for 45 s. Afterward, the unwanted ITO material was dissolved by immersing the sample for 2 min 45 s in an etchant solution (HNO_3/HCl 1:4 (v/v)) under agitation. Finally, an interdigitated electrode structure of square design was obtained (Figure 2B). The cross-linked SU-8 on electrode surfaces is then dissolved in Remover PG (Micro-CHEM).

Transition from a Bipolar to a Quadrupolar Electrode Arrangement Using BDL:

To obtain a quadrupolar electrode matrix, the previously described electrode structure was covered with a thin PDMS insulating layer in which selective openings were formed.

We used a PDMS patterning protocol based on the BDL technique described in ref 31. The process described by Thangawng and coauthors had to be modified and optimized to suit the case of a PDMS film deposited on a glass slide bearing ITO electrodes. The three-step process is summarized in Figure 2C.

Thin PDMS. A thin PDMS film was deposited by spin coating a diluted mixture of 20% PDMS (10:1 prepolymer/cross-linker)/heptane w/w onto the electrode-bearing substrate at 4500 rpm for 60 s. Then, the sample was cured at 80 °C for 2 min 30 s (Figure 2c1). Afterward, the coated substrate was stored at 4 °C to stop cross-linking and avoid hardening of the thin layer. The thickness of the PDMS membrane can be controlled by adjusting the PDMS/heptane ratio as well as spin-coating parameters (see Supporting Information Figure S-1).

Bonding between the PDMS Stamp and the PDMS Membrane. Once the PDMS stamp was peeled off of the mold, a drop of ethanol was placed on the thin PDMS membrane and the stamp patterns were aligned with those of electrodes under a binocular microscope. Ethanol, which is a nonswelling solvent, acts as a lubricant during alignment and delays the bonding process. No pressing force was applied, the weight of the stamp being sufficient to ensure bonding. Assembled devices were then held overnight at 80 °C to evaporate the solvent and complete the bonding process.

Removal of PDMS Insulating Film above the Electrodes. The PDMS stamp was finally peeled off of the electrode-bearing substrate, and the strong adhesion established between the two PDMS surfaces in contact enabled the formation of openings in the PDMS insulating layer. As a result, a 2D electrode grid was obtained with a thin insulating PDMS membrane covering the electrical interconnections between the square conductive pads (Figure 2c3).

Cell and Particle Preparation. Cells. The human embryonic kidney cell line (HEK293, CelluloNet no. 109)³⁶ was obtained from CelluloNet (UMS3444/US8 BioSciences Gerland Lyon-Sud, Lyon, France). Cells were grown at 37 °C under 5% CO_2 in Dulbecco's modified Eagle's medium (high glucose) supplemented with 10% fetal calf serum, 100 $\mu\text{g}/\text{mL}$ streptomycin, and 100 units/mL penicillin.

Before DEP experiments, cells were detached with a trypsin solution (0.05% trypsin/0.02% EDTA in phosphate-buffered saline) and resuspended in a low conductive, isotonic medium. This buffer was obtained by dissolving 5% dextrose (w/v) in DI water before adjusting the conductivity to the desired value with phosphate-buffered saline (PBS). The buffer osmolality was measured using a cryogenic osmometer (Löser, type 6) and found to be equal to 287 mOsm/kg. The solution had a final pH of 7.4.

Microparticles. Carboxylate-modified polystyrene latex particles (3 μm diameter) were purchased from Biovalley (France). Prior to

experiments, latex beads were washed three times with DI water by centrifuging at 8000 rcf for 10 min and resuspended in a KCl solution of 5.7 mS/m conductivity (measured with a Consort C532 conductimeter).

Electric Field Simulations. Three-dimensional electric field calculations were carried out using the ac/dc module of finite element software Comsol Multiphysics 4.3b. Square electrode pads of width 150 μm are connected using 30- μm -wide tracks. The center-to-center distance between two adjacent pads is equal to 400 μm . Figure 5 shows a portion of the electrode array.

The spatial distribution of the electric field strength is represented in Figure 5. Two different electrode configurations were studied. Figure 5A represents the electric field distribution obtained with the bipolar electrode structure (i.e., without insulating material). Figure 5B depicts the spatial distribution of the field obtained with the quadrupolar electrode structure (i.e., with a thin insulating PDMS layer covering the interelectrode space).

Microchip. Particle dielectrophoretic assembly was observed in real time using a long-working-distance optical microscope (Nikon Eclipse, LV 150). The DEP assembly was performed into a 10 μL chamber that consisted of the microchip, an 800- μm -high PDMS spacer delimiting the electrode array, and a thin glass coverslip (Figure 3). The ITO contact pads were connected to an arbitrary waveform generator (Agilent 33250A).

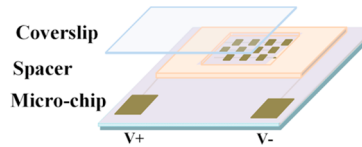


Figure 3. Microchip for dielectrophoretic assembly.

RESULTS AND DISCUSSION

Deposition of the PDMS Layer. First, the deposition of PDMS layers was studied on plain ITO and glass substrates before being studied on the heterogeneous glass/ITO supports. Figure 4 indicates the thickness of PDMS layers spin coated on both uniform substrates for different mass ratios of PDMS/heptane. For the plain glass substrate, the thickness of the deposited layer varied from 1 to 6 μm for PDMS/heptane mass ratios ranging between 10 and 40%, while the thickness of the deposited layer on ITO substrates varied between 100 and 600 nm for the same PDMS/heptane mass ratios. This difference in deposited layer thickness is probably due to the chemical nature of both supports. Angle contact measurements performed on ITO and glass surfaces revealed that ITO is more hydrophobic than glass (see Supporting Information Figure S-2). Therefore, ITO surfaces are more easily wettable by hydrophobic PDMS/heptane solutions than are glass surfaces, allowing a better spreading of the solution and therefore thinner layer deposition. Furthermore, the study of PDMS layer deposition on the ITO/glass surfaces showed results similar to those obtained on plain ITO substrates, which indicates that these heterogeneous substrate surface properties are dominated by their ITO patterns.

Patterning Thin PDMS Layers. The protocol for the patterning of PDMS layers was inspired by BDL.³¹ The direct application of BDL was not suited to our substrate, which consisted of ITO electrodes deposited on glass surfaces. This is due to the plasma treatment step used in the BDL method,³¹ which causes the irreversible adhesion of the thin PDMS layer to the substrate surface, thus impeding the patterning of this layer with PDMS stamps. For this reason, various modifications

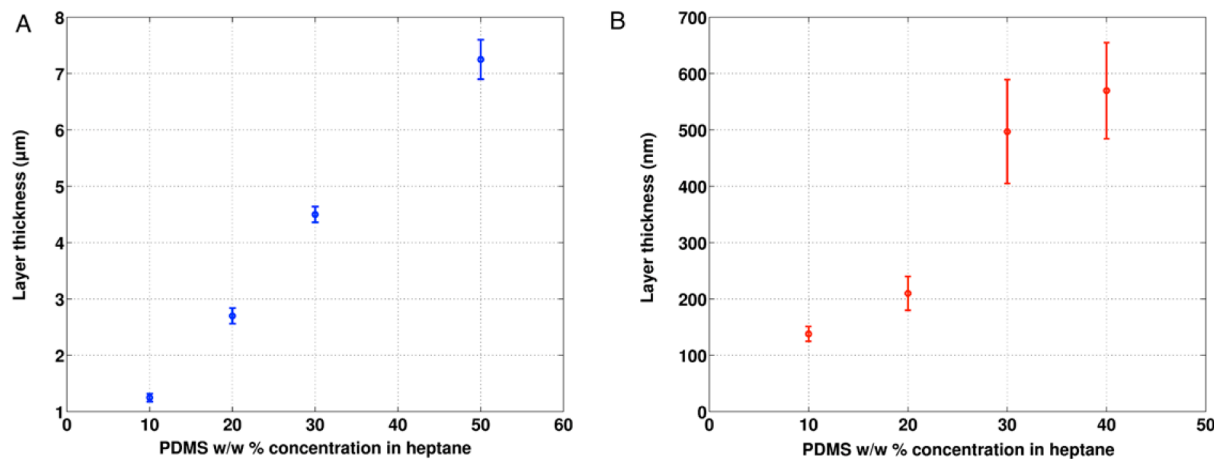


Figure 4. PDMS film thickness for different PDMS w/w % concentrations in heptane for (A) a glass substrate and (B) an ITO substrate. The spin velocity is 4500 rpm, and the duration is 1 min.

and optimizations have been made to reduce the adhesion of the thin layer to the substrate and increase the bonding to PDMS stamps. Therefore, an optimized protocol, with no plasma treatment, has been used. The bonding between the PDMS stamp and the PDMS membrane was promoted by the reticulation phenomenon at their interface. This phenomenon was induced by creating a cross-linker concentration gradient at the interface resulting from the use of two different cross-linker concentrations for preparing PDMS layers (20% w/w) and PDMS stamps (10% w/w). Layers and stamps were cured over a short period of time (60 min) at 80 °C to become hardened enough to handle and remain un-cross-linked enough at the interfaces to form effective bonds. Once the adhesion is achieved between the PDMS thin layer and the stamp, the two parts become irreversibly attached, thereby facilitating the patterning of the layer (Figure 2c2). Irreversible bonds are created between the PDMS layer and PDMS stamp at the interface thanks to the partial cross-linking process. Therefore, the subsequent peeling step induces a localized mechanical stress which enables to tear the PDMS layer only on the contact area. The rest of the PDMS layer remains attached to the glass surface.

Initially, the square pillars on the PDMS stamp had the same dimensions as the ITO square electrodes ($150 \times 150 \mu\text{m}$). However, openings obtained after the peeling step are slightly wider than pillar structures. It is probably due to an increase in the contact surface between the stamp and the PDMS film induced by the collapse of pillar structures during the bonding process. This phenomenon was also observed on the patterns obtained by the BDL method.³¹

Electrical Insulation Using a Thin PDMS Layer.

Different dilution ratios (PDMS/heptane) were tested to obtain the optimal thickness of the insulation PDMS layers. The electrical insulation properties of the patterned PDMS layers were evaluated qualitatively by comparing the dielectrophoretic behavior of particles on the interdigitated electrodes for different layer thicknesses. As shown below, structural assemblies obtained by the dielectrophoretic manipulation of particles change in the presence of the patterned insulation layer on the electrode surface. However, it has been observed that thin PDMS layers were not perfectly insulating when the dilution ratio was lower than 1:4 PDMS/heptane (w/w). The layer thickness above which the coated electrode areas were completely isolated was found to be equal to 200 nm. This

optimal thickness was obtained using a PDMS/heptane dilution ratio of 1:4 (w/w) under processing conditions allowing one to obtain clearly defined PDMS openings.

Electrode Configurations and Electric Field Simulation.

As shown in Figure 5a2, the noninsulated interdigitated

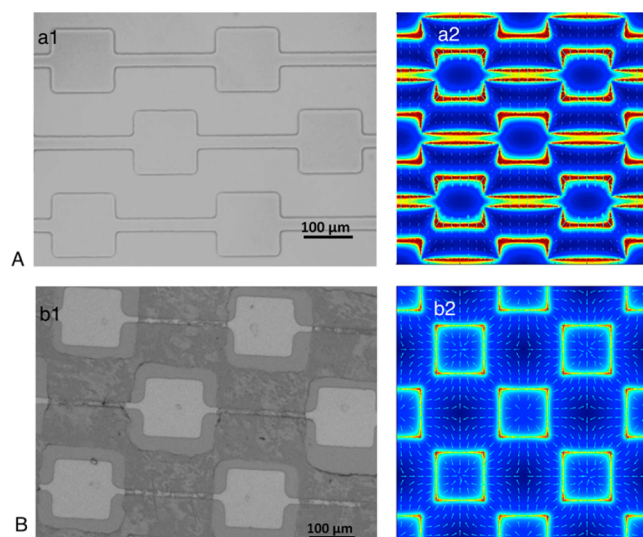


Figure 5. (A) Noninsulated ITO electrodes: (a1) ITO electrodes obtained after chemical wet etching. (a2) Norm of the electric field in the horizontal plane situated $1.5 \mu\text{m}$ above the electrodes ($|E|_{\max} = 1.6 \times 10^8 \text{ V/m}$, $V = 10 \text{ V}_{pp}$). (B) Device after selective isolation using a patterned PDMS film: (b1) ITO conducting structures selectively coated with PDMS. (b2) Electric field simulation in the presence of the insulating layer.

electrode structure produces an electric field that reaches its maxima at the electrode edges (red areas) and its minima in trapezoidal areas located in the interelectrode space. At field frequencies where n-DEP is predominant, particles will therefore be pushed away from the electrodes to these weakest field areas.

The simulation results displayed in Figure 5b2 correspond to the case where the electrode interconnection wires were covered by a thin insulating PDMS film. The electric field distribution is modified accordingly, with a quadrupolar electrode configuration being obtained. As shown in Figure

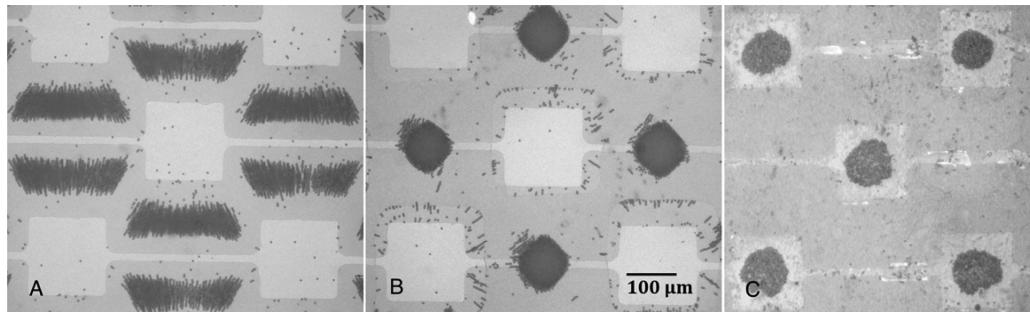


Figure 6. (A) COOH-terminated latex particles ($3\text{ }\mu\text{m}$) assembled by n-DEP using the PDMS-free bipolar structure ($f = 30\text{ kHz}$, 10 V_{pp} , $\sigma_{\text{m}} = 5.7\text{ mS/m}$). (B) Diamond-shaped assemblies obtained with the quadrupolar electrode structure (identical conditions). (C) The ac electroosmotic flow drags the particles toward the electrode centers ($f = 1\text{ kHz}$, $\sigma_{\text{m}} = 5.7\text{ mS/m}$).

5b2, the strongest field areas remain located at the electrode edges, but the field minima now correspond to the centers of each quadrupolar electrode set.

Dielectrophoretic Assembly of Polystyrene Latex Beads. The dielectrophoretic behavior of $3\text{ }\mu\text{m}$ carboxylate-modified latex particles was investigated at different frequencies in DI water and in a KCl medium of conductivity 5.7 mS/m , with both bipolar and quadrupolar electrode structures. When a 10 V_{pp} signal was applied, in the case of particles immersed in water, p-DEP was observed between 10 and 20 kHz , while beads were systematically repelled from the electrodes by n-DEP above 60 kHz . The crossover frequency, at which the DEP force canceled, was therefore between 20 and 60 kHz . Below 10 kHz , ac electroosmosis effects also arose, due to the interaction of the electric field with the charge at the electrode surface. This resulted in bead transport by the flow toward the electrode center.

When beads were immersed in a KCl medium of conductivity 5.7 mS/m , they were similarly dragged toward the electrode center by the electroosmotic flow (Figure 6C) for frequencies lower than 10 kHz (which was even more noticeable around 1 kHz). However, only n-DEP was observed above 10 kHz . The microparticles experienced a force aligning them along the electric field lines and directing them toward the weakest electric field areas to form regularly spaced trapezoidal and diamond-shaped assemblies using the bipolar and quadrupolar structures, respectively (Figure 6A,B). They were repelled toward the interelectrode space within a few seconds, but strongly assembled clusters were obtained after approximately 10 min . The compactness of the formed clusters also depended on the applied voltage (see Supporting Information Figure S-3). The results shown in Figure 6A,B are in close agreement with the electric field simulations, with the weakest field areas presenting the same shape as the particle clusters. These results confirm that the patterned PDMS film functions properly as an electrical insulation layer, allowing the fabrication of a quadrupolar electrode matrix.

The bead response to the ac electric field can be interpreted by studying the $Re[\text{CM}]$ factor, which is mostly determined in the low-frequency range by particle and medium conductivities. As previously mentioned, the latex particle conductivity is mainly related to the surface conductance. In DI water, K_s^d , which is proportional to $(c)^{1/2}$ (eqs 6 and 7), can be neglected, and K_s^i can therefore be deduced from eq 4. Since the DEP crossover frequency is between 20 and 60 kHz , the value of σ_p can be estimated to be in the range of 1.20×10^{-4} to $3.64 \times 10^{-4}\text{ S/m}$, according to eqs 2 and 3, in which $Re[\text{CM}]$ is set equal to 0. K_s^i is therefore in the range 9×10^{-11} to $2.73 \times$

10^{-10} S . It can be noticed that this result is close to the value reported by Suzuki et al. for $3\text{ }\mu\text{m}$ latex microparticles with amino terminal groups.

When the medium conductivity is increased to 5.7 mS/m , the contribution of the diffuse layer conductance to the total surface conductance becomes more significant. The zeta potential of $3\text{ }\mu\text{m}$ carboxylate-modified latex particles was measured with a Zetasizer Nano ZS analyzer (Malvern Instruments) and found to be equal to -78 mV , which leads to a K_s^d value of $3.64 \times 10^{-10}\text{ S}$. Moreover, K_s^i can be considered to be unchanged with respect to its value in water.³⁷ This gives a value of between 4.54×10^{-10} and $6.37 \times 10^{-10}\text{ S}$ for K_s , leading to a σ_p value of between 6.05×10^{-4} and $8.49 \times 10^{-4}\text{ S/m}$.

The corresponding average plots of $Re[\text{CM}]$ for particles suspended in water and in 5.7 mS/m KCl are given Figure 7.

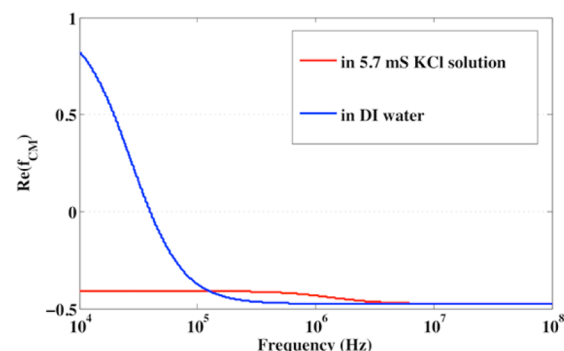


Figure 7. $Re[\text{CM}]$ as a function of frequency and immersion medium for a $3\text{-}\mu\text{m}$ -diameter carboxyl-terminated polystyrene latex sphere ($\epsilon_p = 2.56$, $\epsilon_m = 78$).

They enable us to predict the DEP behavior of latex beads with respect to frequency and are consistent with the experimental observations. In particular, latex beads immersed in the 5.7 mS KCl solution experienced n-DEP only above 10 kHz , as could be expected from the plot showing a negative value of $Re[\text{CM}]$. The value of $Re[\text{CM}]$ at a given frequency can be used to calculate the DEP force exerted on a particle at each location from eq 1 using Comsol Multiphysics (see Supporting Information Figure S-4).

Dielectrophoretic Assembly of HEK Cells. DEP assembly of HEK 293 cells was also studied using the fabricated quadrupolar electrode array. Cell dielectrophoretic behavior in a specific medium and at a given frequency can be predicted by calculating the CM factor. According to the single-shell

dielectric model developed by Irimajiri,³⁸ the cell complex permittivity can be related to the cell area-specific membrane capacitance and conductance C_m and G_m , conductivity, relative permittivity of the cell interior σ_{int} and ϵ_{int} , and cell radius r . The variation of the CM factor could therefore be determined as a function of frequency and medium conductivity from previously reported HEK cell electric parameters^{39,40} (Figure 8).

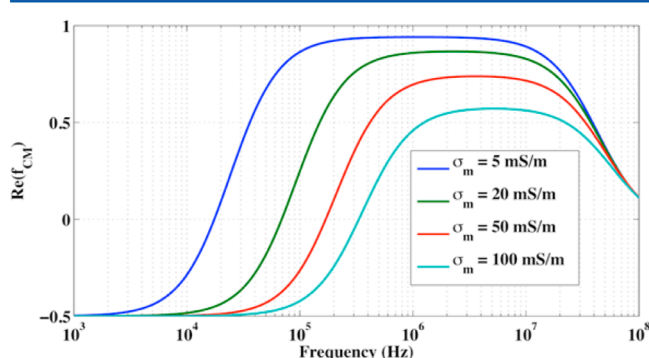


Figure 8. $Re(f_{CM})$ as a function of frequency and medium conductivity for a 15- μm -diameter HEK cell ($C_m = 8.5 \text{ fF}/\text{m}^2$, $G_m \approx 0 \text{ S}/\text{m}^2$, $\sigma_{int} = 533 \text{ mS}/\text{m}$, and $\epsilon_{int} = 71$). A buffer relative permittivity of 78 was used.

DEP assembly by nDEP was performed in a buffer of conductivity 50 mS/m. This value is sufficiently low to prevent Joule heating and sufficiently high to give the maximum possible value of $Re[CM]$ (-0.5) at 20 kHz. At this frequency, electroosmotic effects can be assumed to be negligible. Under those conditions (and for a 10 V_{pp} applied voltage), HEK cells were indeed submitted to negative DEP and formed aggregates located at electric field minima (Figure 9A,B). The collection time was also studied with respect to the applied voltage (see Supporting Information Figure S-5). Above 180 kHz, cells were attracted toward electrode edges by pDEP (Figure 9C). These results are consistent with the red plot in Figure 8 ($Re[CM]$ versus f for $\sigma_m = 50 \text{ mS}/\text{m}$).

We have reported a new process for fabricating DEP devices using thin micropatterned PDMS films combined with simple electrodes. It is also worth mentioning that the same microchip can be used in many experiments, as the thin PDMS layer is quite resistant to cleaning (ethanol, acetone, and sonication were tested). When needed, the thin PDMS layer can also be removed by gentle rubbing with a heptane-impregnated tissue, allowing further reuse of ITO electrodes. The proposed process is therefore economical and has a limited impact on the environment. Modifying electrode and/or stamp patterns should also allow us to obtain particle clusters of various shapes.

CONCLUSIONS

We have proposed a new approach to fabricating matrices of quadrupolar electrodes dedicated to the dielectrophoretic assembly of a wide range of colloids. For this purpose, we have developed a process to perform selective openings in PDMS membranes covering ITO surfaces, based on bonding and detaching PDMS. The patterned PDMS film was used as an insulator, which allowed the conversion of a bipolar electrode arrangement to an array of quadrupolar electrode sets. The processing steps are simple and do not require expensive equipment. Only a laminar flow hood equipped with a spin-coater and a small UV lamp were needed. Moreover, the PDMS stamp mold can be reused many times.

PDMS proved efficient as a patternable insulating material. This was confirmed experimentally by performing the assembly of latex polystyrene beads using nDEP in the presence and absence of the PDMS membrane. Fully biocompatible and transparent, the chip presented in this article offers an interesting potential for cell culture and tissue-engineering applications.

ASSOCIATED CONTENT

S Supporting Information

PDMS film thickness versus rotation speed. Contact angle measurements confirming that ITO surfaces are more wettable than glass surfaces. nDEP assembly of 3 μm COOH polystyrene microspheres with quadrupolar electrodes. DEP force simulation. nDEP assembly of HEK293 cells suspended in a 5% dextrose medium. This material is available free of charge via the Internet at <http://pubs.acs.org>.

AUTHOR INFORMATION

Corresponding Authors

*E-mail: naoufel-haddour@ec-lyon.fr. Tel: +33 4 72 18 61 12.
*E-mail: marie.robin@univ-lyon1.fr. Tel: +33 4 72 18 61 12.

Present Address

N.H. and M.F.-R.: 36 Avenue Guy de Collongue, 69130 Écully, France

Notes

The authors declare no competing financial interest.

ACKNOWLEDGMENTS

We thank the French Ministry of Research for funding S.M.'s Ph.D. grant. We acknowledge the contribution of the CelluloNet facility of UMS3444/US8 Biosciences Gerland-Lyon Sud. We also thank Laure Franqueville for her valuable advice and guidance regarding cell culture work as well as Pierre Cremillieu and Radoslaw Mazurczyk for their support with the NanoLyon technological platform.

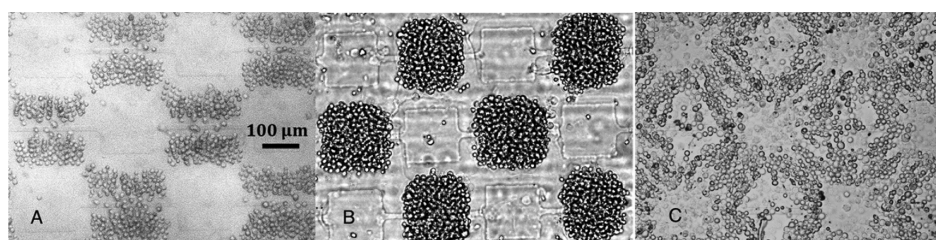


Figure 9. (A) Bipolar electrodes: nDEP assembly of HEK cells ($f = 20 \text{ kHz}$, $\sigma_m = 51.2 \text{ mS}/\text{m}$). (B, C) Observation of nDEP and pDEP with quadrupolar electrodes at 20 and 200 kHz, respectively (same buffer conductivity).

ABBREVIATIONS

PDMS: poly(dimethylsiloxane); DEP: dielectrophoresis; ITO: indium tin oxide; HEK: human embryonic kidney; CMF: Clausius–Mossotti factor

REFERENCES

- (1) Pohl, H. A. *Dielectrophoresis*; Cambridge University Press: Cambridge, U.K., 1978.
- (2) Gray, D. S.; Tan, J. L.; Voldman, J.; Chen, C. S. Dielectrophoretic Registration of Living Cells to a Microelectrode Array. *Biosens. Bioelectron.* **2004**, *19*, 1765–1774.
- (3) Velev, O. D.; Kaler, E. W. In Situ Assembly of Colloidal Particles into Miniaturized Biosensors. *Langmuir* **1999**, *15*, 3693–3698.
- (4) Green, N. G.; Morgan, H. Dielectrophoresis of Submicrometer Latex Spheres. 1. Experimental Results. *J. Phys. Chem. B* **1999**, *103*, 41–50.
- (5) Hughes, M. P.; Green, N. G. The Influence of Stern Layer Conductance on the Dielectrophoretic Behavior of Latex Nanospheres. *J. Colloid Interface Sci.* **2002**, *250*, 266–268.
- (6) Zhang, C.; Khoshmanesh, K.; Tovar-Lopez, F. J.; Mitchell, a.; Wlodarski, W.; Klanter-zadeh, K. Dielectrophoretic Separation of Carbon Nanotubes and Polystyrene Microparticles. *Microfluid. Nanofluid.* **2009**, *7*, 633–645.
- (7) Benson, O. Assembly of Hybrid Photonic Architectures from Nanophotonic Constituents. *Nature* **2011**, *480*, 193–199.
- (8) Yang, L.; Banada, P. P.; Chatni, M. R.; Seop Lim, K.; Bhunia, A. K.; Ladisch, M.; Bashir, R. A Multifunctional Micro-Fluidic System for Dielectrophoretic Concentration Coupled with Immuno-Capture of Low Numbers of Listeria Monocytogenes. *Lab Chip* **2006**, *6*, 896–905.
- (9) Crews, N.; Darabi, J.; Voglewede, P.; Guo, F.; Bayoumi, A. An Analysis of Interdigitated Electrode Geometry for Dielectrophoretic Particle Transport in Micro-Fluidics. *Sens. Actuators, B* **2007**, *125*, 672–679.
- (10) Ermolina, I.; Morgan, H. The Electrokinetic Properties of Latex Particles: Comparison of Electrophoresis and Dielectrophoresis. *J. Colloid Interface Sci.* **2005**, *285*, 419–428.
- (11) Arnold, W. M.; Schwan, H. P.; Zimmermann, U. Surface Conductance and Other Properties of Latex Particles Measured by Electrorotation. *J. Phys. Chem.* **1987**, *91*, 5093–5098.
- (12) Hughes, M. P. Computer-Aided Analysis of Conditions for Optimizing Practical Electrorotation. *Phys. Med. Biol.* **1998**, *43*, 3639–3648.
- (13) Jones, T. B. Basic Theory of Dielectrophoresis and Electrorotation. *IEEE Eng. Med. Biol. Mag.* **2003**, *22*, 33–42.
- (14) Huang, Y.; Pethig, R. Electrode Design for Negative Dielectrophoresis. *Meas. Sci. Technol.* **1991**, *2*, 1142.
- (15) Yu, Z.; Xiang, G.; Pan, L.; Huang, L.; Yu, Z.; Xing, W.; Cheng, J. Negative Dielectrophoretic Force Assisted Construction of Ordered Neuronal Networks on Cell Positioning Bioelectronic Chips. *Biomed. Microdev.* **2004**, *6*, 311–324.
- (16) Frénáea, M.; Faure, S. P.; Le Pioufle, B.; Coquet, P.; Fujita, H. Positioning Living Cells on a High-Density Electrode Array by Negative Dielectrophoresis. *Mater. Sci. Eng., C* **2003**, *23*, 597–603.
- (17) Huang, Y.; Rubinsky, B. Microfabricated Electroporation Chip for Single Cell Membrane Permeabilization. *Sens. Actuators, A* **2001**, *89*, 242–249.
- (18) Grilli, S.; Ferraro, P. Dielectrophoretic Trapping of Suspended Particles by Selective Pyroelectric Effect in Lithium Niobate Crystals. *Appl. Phys. Lett.* **2008**, *92*, 232902.
- (19) Gennari, O.; Grilli, S.; Coppola, S.; Pagliarulo, V.; Vespini, V.; Coppola, G.; Bhowmick, S.; Gentile, G.; Ambrogi, V.; Cerruti, P.; et al. Through Surface Charge Templates. *Langmuir* **2013**, *29*, 15503–15510.
- (20) Judy, J. W. Microelectromechanical Systems (MEMS): Fabrication, Design and Applications. *Smart Mater. Struct.* **2001**, *10*, 1115–1134.
- (21) Yuen, P. K.; Su, H.; Goral, V. N.; Fink, K. a. Three-Dimensional Interconnected Microporous Poly(dimethylsiloxane) Microfluidic Devices. *Lab Chip* **2011**, *11*, 1541–1544.
- (22) Sia, S. K.; Whitesides, G. M. Microfluidic Devices Fabricated in Poly (Dimethylsiloxane) for Biological Studies. *Electrophoresis* **2003**, *24*, 3563–3576.
- (23) Shafiee, H.; Caldwell, J. L.; Sano, M. B.; Davalos, R. V. Contactless Dielectrophoresis: A New Technique for Cell Manipulation. *Biomed. Microdev.* **2009**, *11*, 997–1006.
- (24) Schneider, F.; Draheim, J.; Kammerer, R.; Wallrabe, U. Process and Material Properties of Polydimethylsiloxane (PDMS) for Optical MEMS. *Sens. Actuators, A* **2009**, *151*, 95–99.
- (25) Park, J.; Kim, H.; Han, A. Micropatterning of Poly (dimethylsiloxane) Using a Photoresist Lift-off Technique for Selective Electrical Insulation of Microelectrode Arrays. *J. Micromech. Microeng.* **2009**, *19*, 1–18.
- (26) Ryu, K. S.; Member, S.; Wang, X.; Shaikh, K.; Liu, C.; Member, S. A Method for Precision Patterning of Silicone Elastomer and Its Applications. *J. Microelectromech. Syst.* **2004**, *13*, 568–575.
- (27) Tserepi, a.; Cordoyiannis, G.; Patsis, G. P.; Constantoudis, V.; Gogolides, E.; Valamontes, E. S.; Eon, D.; Peignon, M. C.; Cartry, G.; Cardinaud, C.; et al. Etching Behavior of Si-Containing Polymers as Resist Materials for Bilayer Lithography: The Case of Poly-Dimethyl Siloxane. *J. Vac. Sci. Technol., B* **2003**, *21*, 174.
- (28) Tong, J.; Simmons, C. a.; Sun, Y. Precision Patterning of PDMS Membranes and Applications. *J. Micromech. Microeng.* **2008**, *18*, 037004.
- (29) Bhagat, A. A. S.; Jothimuthu, P.; Papautsky, I. Photodefinable Polydimethylsiloxane (PDMS) for Rapid Lab-on-a-Chip Prototyping. *Lab Chip* **2007**, *7*, 1192–1197.
- (30) Grilli, S.; Vespini, V.; Ferraro, P. Surface-Charge Lithography for Direct PDMS Micro-Patterning. *Langmuir* **2008**, *24*, 13262–13265.
- (31) Thangawng, A. L.; Swartz, M. a.; Glucksberg, M. R.; Ruoff, R. S. Bond-Detach Lithography: A Method for Micro/nanolithography by Precision PDMS Patterning. *Small* **2007**, *3*, 132–138.
- (32) Pethig, R. Review Article-Dielectrophoresis: Status of the Theory, Technology, and Applications. *Biomicrofluidics* **2010**, *4*, 1–35.
- (33) Hughes, M. P. *Nanoelectromechanics in Engineering and Biology*; CRC Press: Boca Raton, FL, 2003.
- (34) Suzuki, M.; Yasukawa, T.; Mase, Y.; Oyamatsu, D.; Shiku, H.; Matsue, T. Dielectrophoretic Micropatterning with Microparticle Monolayers Covalently Linked to Glass Surfaces. *Langmuir* **2004**, *20*, 11005–11011.
- (35) Lyklema, J. *Fundamentals of Interface and Colloid Science*; Academic Press: London, 1995.
- (36) Graham, F. L.; Smiley, J.; Russell, W. C.; Nairn, R. Characteristics of a Human Cell Line Transformed by DNA from Human Adenovirus Type 5. *J. Gen. Virol.* **1977**, *36*, 59–72.
- (37) Hughes, M.; Morgan, H.; Flynn, M. The Dielectrophoretic Behavior of Submicron Latex Spheres: Influence of Surface Conductance. *J. Colloid Interface Sci.* **1999**, *220*, 454–457.
- (38) Irimajiri, A.; Hanai, T.; Inouye, A. A Dielectric Theory of “Multi-Stratified Shell” Model with Its Application to a Lymphoma Cell. *J. Theor. Biol.* **1979**, *78*, 251–269.
- (39) Zimmermann, D.; Kiesel, M.; Terpitz, U.; Zhou, a.; Reuss, R.; Kraus, J.; Schenk, W. a.; Bamberg, E.; Sukhorukov, V. L. A Combined Patch-Clamp and Electrorotation Study of the Voltage- and Frequency-Dependent Membrane Capacitance Caused by Structurally Dissimilar Lipophilic Anions. *J. Membr. Biol.* **2008**, *221*, 107–121.
- (40) El-Gaddar, A.; Frénáea-Robin, M.; Voyer, D.; Aka, H.; Haddour, N.; Krähenbühl, L. Assessment of 0.5 T Static Field Exposure Effect on Yeast and HEK Cells Using Electrorotation. *Biophys. J.* **2013**, *104*, 1805–1811.